Technical Notes

New Data Reduction Equation for Diamond Slug Calorimeter Heat Transfer Gauges

J. I. Frankel*
New Mexico State University,
Las Cruces, New Mexico 88003
Rowland T. Penty Geraets† and M. McGilvray‡
University of Oxford,
Oxford, England OX1 2JD, United Kingdom
and
Hongchu Chen§
Rheem Corporation, Montgomery, Alabama 36109

https://doi.org/10.2514/1.T6021

Nomenclature

A	=	cross-sectional area, m^2
a_1	=	constant, $J/(m^2 \cdot K)$
c	=	specific heat capacity, $J/(kg \cdot K)$
k	=	thermal conductivity, $W/(m \cdot K)$
L_1, L_2	=	lengths, m
M_f	=	multiplication factor
M_1	=	kernel, $(m^2 \cdot K)/W$
m	=	discrete regularization parameter
N	=	number of data points beyond the initial condition
$q_{o''}$	=	maximum heat flux, W/m^2
$q_{s''}$	=	source heat source, W/m^2
$\hat{q}_{s''}$	=	approximate source heat source, W/m^2
q''	=	heat flux, W/m^2
$R(dq''/dt)$	=	cross-correlation coefficient for heat flux rate
$R(q'')$	=	cross-correlation coefficient for heat flux
T	=	temperature, °C
T_o	=	initial temperature, °C
t	=	time, s
u	=	dummy time variable, s
x	=	spatial coordinate, m
β	=	thermal effusivity, $(W \cdot \sqrt{s})/(m^2 \cdot K)$
γ_m	=	future-time parameter, s
Δt	=	time sampling intervals, s
δ	=	thickness of thin-film sensor, m
θ	=	reduced temperature; $T - T_o$, °C, K
$\bar{\theta}$	=	average reduced temperature, °C, K
ρ	=	density, kg/m^3

Received 6 February 2020; revision received 8 July 2020; accepted for publication 3 August 2020; published online 28 August 2020.

*Department Head and R. Myers Endowed Professor, Mechanical and Aerospace Engineering Department. Associate Fellow AIAA.
†D.Phil. Candidate, Department of Engineering Sciences.
‡Associate Professor, Department of Engineering Sciences.
§Research Engineer.

I. Introduction

THIS Note applies an alternative data reduction equation for reconstructing the surface heat flux for a diamond slug calorimeter for use in short-duration impulse flow facilities [1]. Calorimeter gauges have been used in shock tube studies [2,3] for estimating heat flux. The heat flux gauge consists of a thin layer of synthetic diamond (produced using chemical vapor deposition) with a thin-film resistance temperature detector (RTD) sputtered on its rear surface to measure temperature rise. Previous methods for analyzing the measured data from this style of gauge can be found in Refs. [1,4] and the classical Schultz and Jones [5] AGARD report. These methods serve as a baseline in developing the preconditioned integral equation previously published by Frankel et al. [6] and Frankel and Chen [7].

There are many benefits for applying the integral form for data reduction in calculating heat flux from this type of gauge. These include no errors due to spatial discretization; minimizing processing time without sacrificing accuracy; regularization easily incorporated to promote stability; and physical-based preconditioning of the data, which removes the need for prefiltering of the raw data and preserves energy considerations. This method can be easily coupled to thermal-phase plane and cross-correlation analyses to select the optimal regularization parameter.

This technical Note illustrates the approach and uses a numerical study to compare the estimated solution to the exact solution for a pulse of heat flux that represents a measurement in a reflected shock tunnel. The accuracy and stability of the solution are investigated both with a noise-free temperature signal and with the addition of representative experimental measurement noise.

II. Formulation

Figure 1a shows the idealized one-dimensional representation of the sensor; whereas Fig. 1b displays the reduced model used in this Note, where the thin film has been removed. This assumes negligible Ohmic heating and energy storage in the RTD film, which is valid for the gauge investigated here. Adiabatic side conditions are imposed, and perfect thermal contact is assumed between each of the layers. The substrate material is composed of a thermal insulator. Constant thermophysical properties are assumed, which are valid for short-duration testing where the temperature rises are small, and thus specific heat capacity and thermal conductivity changes of the diamond layer are negligible [6].

Figure 1c displays the exploded model for the lumped-diamond distributed-slug substrate (L-D) formulation. The temperature at the RTD location $\theta_1(L_1, t)$ is assumed to be equal to the average temperature $\bar{\theta}_1(t)$ (i.e., the diamond [8] is isothermal). When the thermophysical properties of the system are constant, the lumped, physically formed variable is mathematically equivalent to the average temperature. The validity of this assumption is explored in the Results section (Sec. III) of this Note. The energy balance per unit cross-sectional area in region 1 is

$$q_s''(t) = q''_{\text{out},1}(t) + \rho_1 c_1 L_1 \frac{d\bar{\theta}_1}{dt}(t), \qquad t \geq 0 \tag{1}$$

Equation (1) is equivalent to that presented in equation 6b in the work of Frankel and Chen [7], which presented a data reduction equation for a thin-film heat transfer gauge on a semi-infinite substrate with significant thermal storage in the film. As the models and assumptions are similar, the same analysis can be applied here, leading to the following preconditioned data reduction equation:

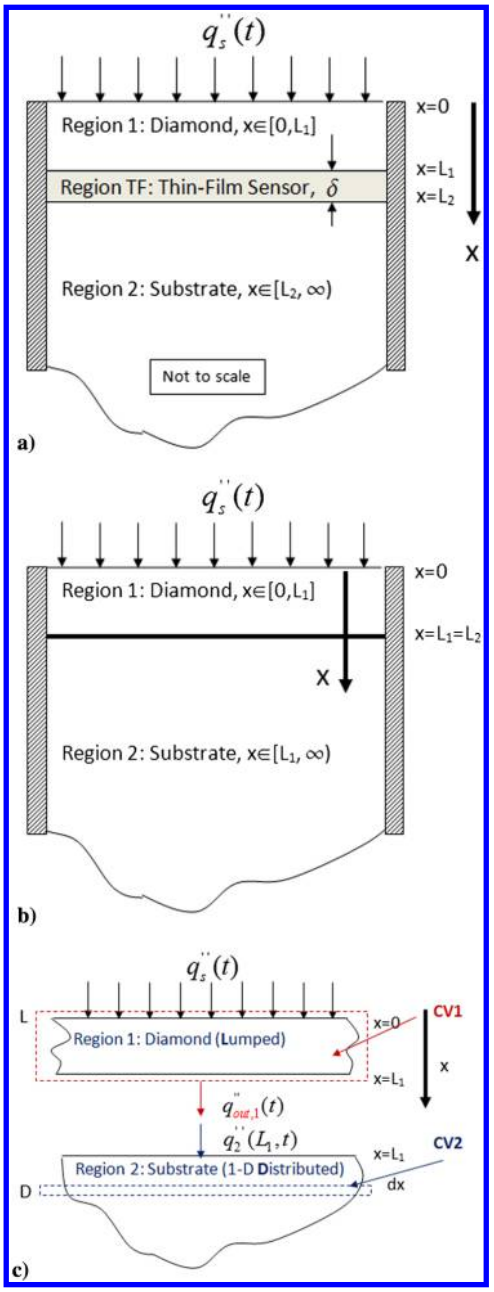

Fig. 1 Schematic of the diamond heat transfer gauge for a) idealized sensor, b) simplified model, and c) exploded view for the lumped formulation (L-D). (1-D denotes one-dimensional.)

$$\int_{u=0}^{t} \theta_1(L_1,u)\,\mathrm{d}u = \int_{u=0}^{t} \hat{q}_s''(u) M_1(t-u)\,\mathrm{d}u, \qquad t \geq 0 \tag{2}$$

where the kernel $M_1(t-u)$ is defined as

$$M_1(t-u) = \frac{a_1}{\beta_2^2}\left(-1 + 2\frac{\beta_2}{a_1}\sqrt{\frac{t-u}{\pi}} + e^{(\beta_2/a_1)^2(t-u)}\right) \times \operatorname{erfc}\left(\frac{\beta_2}{a_1}\sqrt{t-u}\right), \qquad (t-u) \geq 0 \tag{3}$$

where $a_1 = \rho_1 c_1 L_1$, and $\beta_2 = \sqrt{\rho_2 c_2 k_2}$. The approximation that $\hat{q}_s''(t) \approx q_s''(t)$ could be explored further to investigate the bias introduced by using the single-point temperature at $x = L_1$, but it will not be explored here. The preconditioner, of which more details can be found in Ref. [7], acts as a first-pass parameter-free low-pass filter operating on the *functional equation*. This is different than prefiltering data and then inserting the smoothed values into the functional equation. Prefiltering data requires a cutoff frequency or some other criteria to be defined. Furthermore, prefiltering data for substitution disturbs the balance of the functional equation, and hence it loses the equal sign. The preconditioner used here preserves the equal sign (energy balance) as it operates on both the data and heat flux/kernel.

The computational procedure for solving these equations is well described in Ref. [7]. As Eq. (2) is ill-posed, regularization is required to ensure stability [9]. While the preconditioner has a stabilizing effect and allows for easier identification of the optimum regularization parameter, as will be seen in the subsequent section, additional regularization is required to ensure stability in the prediction to Eq. (2). This work applies regularization using the future-time method, with a regularization parameter that is a multiple of the temporal discretization time step ($\gamma_m = mM_f\Delta t$, where m and M_f are both integers) [7]. The value of the regularization parameter should be chosen to meet stability requirements without oversmoothing the solution. In this Note, two methods (which are described in detail in Ref. [10]) are applied to identify the optimal regularization parameter: the thermal-phase plane analysis method, and the cross-correlation coefficient method.

III. Results

A synthetic heat flux profile is formulated based on a typical measurement on a stagnation probe in a reflected shock tunnel experiment. Table 1 provides the parameters considered in the study, including material properties and dimensions of the gauge. The chosen demonstrative heat flux case is defined by the severe discontinuous pulse of heat flux:

$$q_s''(t) = \begin{cases} 0, & 0 \leq t < 250\ \mu\mathrm{s}; \\ q_o'', & 250\ \mu\mathrm{s} \leq t \leq 2250\ \mu\mathrm{s}; \\ 0, & 2250\ \mu\mathrm{s} < t \leq 2500\ \mu\mathrm{s} \end{cases} \tag{4}$$

The heat flux $q_s''(t)$ was imposed as the driving source condition for the lumped slug model of the gauge. The initial condition of gauge is $\bar{\theta}(0) = 0$, whereas the initial condition of the substrate is $\theta_2(x,0) = 0, L_1 \leq x \leq \infty$. Figures 2a and 2b illustrate, respectively, the temperature history and difference between the average temperature of the diamond layer $\bar{\theta}_1(t)$ and the backside temperature at the RTD location $\theta_1(L_1,t)$. These results are easily and analytically available by solving the distributed problem involving two partial differential equations (regions 1 and 2) that follow the Laplace transform methodology described in Ref. [5].

The maximum temperature rise is 5 K, which would alter the actual specific heat capacity of diamond by 4%, which justifies the assumption of constant thermophysical properties in the model. The maximum temperature difference between the average temperature and the back surface temperature is ≈40 mK.

Table 1 Simulation parameters

Parameter/property	Value	Units
c – substrate	790	J/(kg · K)
c – diamond	495	J/(kg · K)
ρ – substrate	2520	kg/m^3
ρ – diamond	3514	kg/m^3
k – substrate	1.46	W/(m · K)
k – diamond	1000	W/(m · K)
L_1	200	μm
Δt	5	μs
M_f	1	——
T_o	293.15	K
q_o''	1	MW/m^2

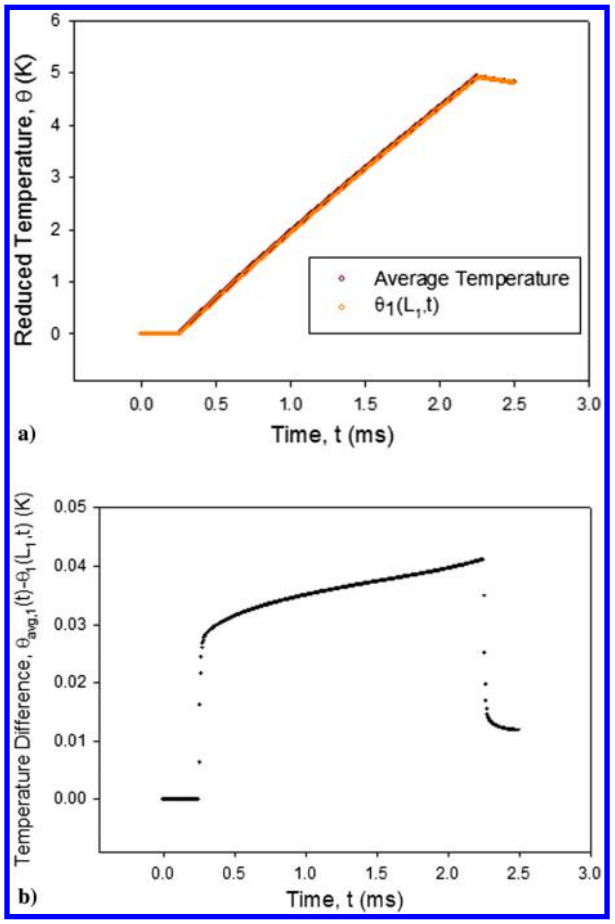

Fig. 2 Results from analytic simulation of the heat flux profile: a) temperature histories, and b) temperature differences.

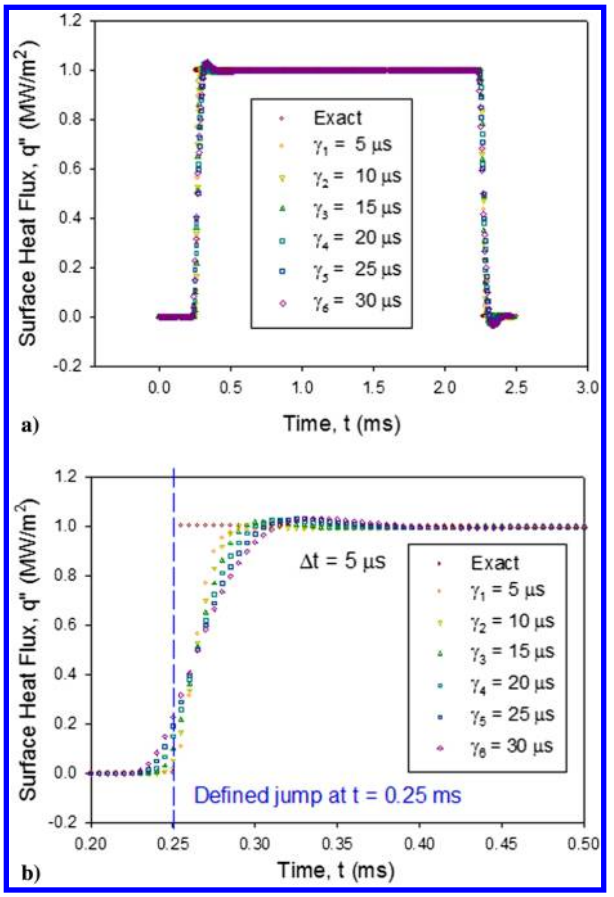

Fig. 3 Heat flux predictions over the regularization spectrum for a) the preconditioned formulation using the ideal data presented in Fig. 2a and b) zoomed-in region near the step condition.

To show the numerical accuracy of the alternative data reduction equation for reconstructing the surface heat flux, a noise-free solution is investigated. Solutions for a range of regularization parameters are shown in the range of $m = 1$–6, resulting in $\gamma_m = 5$–30 μs, and presented in Figs. 3a and 3b. Apart from at the discrete steps, the method is shown to replicate the heat flux profile. As expected at the step, spreading effects occur as the regularization parameter increases, and overshooting Gibb-like phenomena [11] are seen. Recall that the average temperature physically changes value before the slug's backside temperature at $x = L_1$ due to thermal penetration effects.

To quantify the error in the method, the difference between the applied heat flux and the predicted heat flux for $\gamma_1 = 5$ μs is shown in Fig. 4. The error is seen to reduce to below 1% within 50 μs, and the minimum difference is seen to be 0.26%. This result is in line with expectations because the response time of the gauge as an ideal calorimeter based on the analysis of Schultz and Jones [5] is approximately 40 μs.

To investigate the effect of temperature measurement noise on the stability and accuracy of the method, white noise was superimposed with a peak-to-peak amplitude of 5 mK. This level of noise is in expectation of the physical device [4]; however, the power-spectral density is constant with frequency, intentionally representing an extreme case to illustrate the merit of the preconditioned formulation.

Figure 5 presents a family of surface heat flux predictions over a spectrum of regularization parameters for the preconditioned formulation using the noisy temperature data. It is clear that the predicted heat flux signal is much noisier than the previous heat flux predictions calculated from noise-free data. The fluctuations in heat flux are seen to decrease with increasing values of the regularization parameter, although the same spreading effects are seen at the step changes, as seen more clearly in Fig. 6. All values still predict the overall behavior of the input heat flux. The root-mean-squared error (RMSE) from the preconditioned solution to the prescribed heat flux is a minimum at a

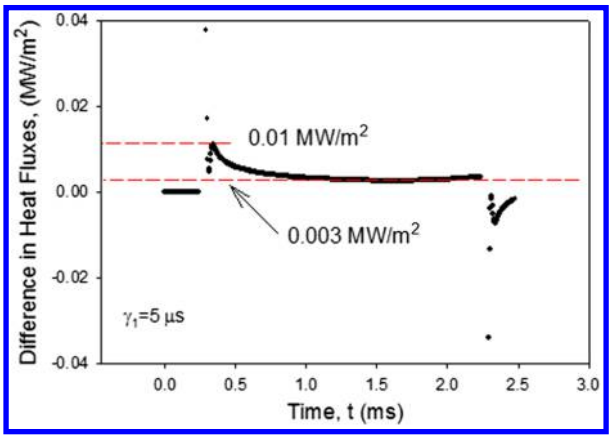

Fig. 4 Difference between the applied heat flux and the predicted heat flux for $\gamma_1 = 5$ μs.

regularization parameter of $\gamma = 20$ μs, although it is insensitive over the range $\gamma = 15$–25 μs. Although the RSME is useful in predicting the optimal regularization parameter for this synthetic case, in a real experiment, it cannot be calculated because the input heat flux is unknown.

Figures 7 and 8 present the thermal-phase plane and cross-correlation phase plane, respectively, to guide the optimal choice of the regularization parameter. See Refs. [7,10] for more detail regarding these methods. The onset of a clear pattern in the thermal-phase plane provides a qualitative indicator of optimality [10], seen at $\gamma = 15$–20 μs. The cross-correlation phase plane is used to identify the optimal regularization parameter by plotting regularized pairings of the cross-correlation coefficient heat flux rate $[R(dq''/dt)]$ against

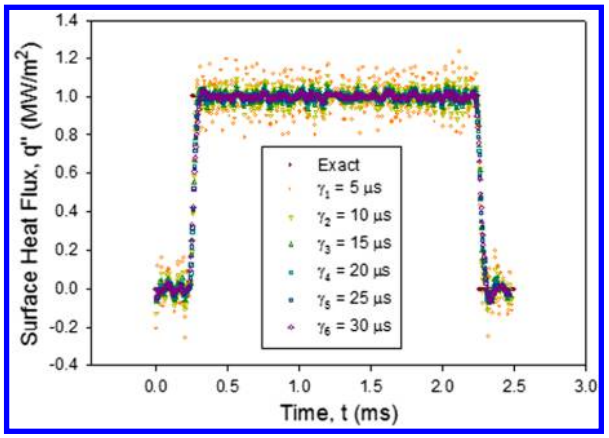

Fig. 5 Heat flux predictions over the regularization spectrum for preconditioned formulations.

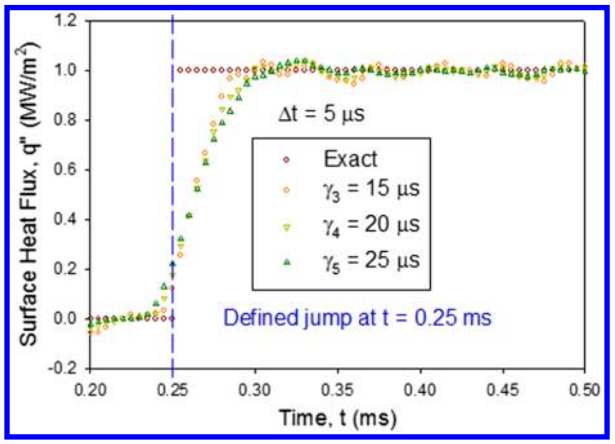

Fig. 6 A zoomed-in view of the heat flux predictions (Fig. 5) near the jump condition at $t = 0.25$ ms for the preconditioned formulation for $\gamma = 15$–25 μs.

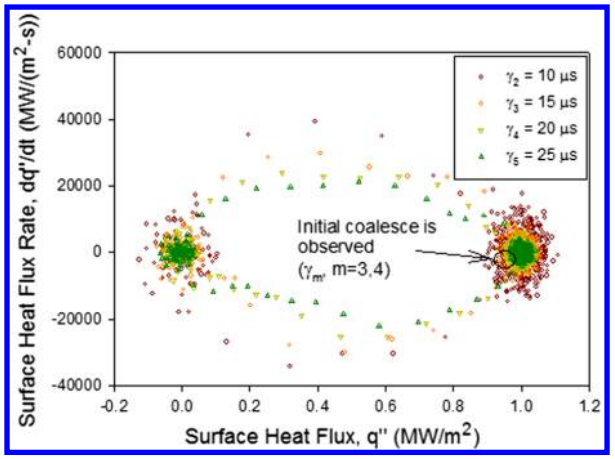

Fig. 7 Thermal-phase plane phase plane for the noisy results.

the cross-correlation coefficient heat flux $[R(q'')]$. A transition between instability-dominated error and error due to oversmoothing is seen to occur at $R(dq''/dt) \approx 0.75$, i.e., for the solutions in the range $\gamma = 15$–25 μs. Irrespective of using the "cusp" condition of $R(dq''/dt) \approx 0.75$, a clear trend is indicated by the line drawn in the optimality/oversmoothing regions. This characteristic behavior is similar to what is used in other techniques, (for example, L-curve analysis [12]). Encouragingly, both of these methods predict optimal regularization parameter in the same range and as calculated from the RMSE. Figure 8 shows a zoomed-in view of these three selected heat flux solutions near the jump heat flux condition at $t = 0.25$ ms.

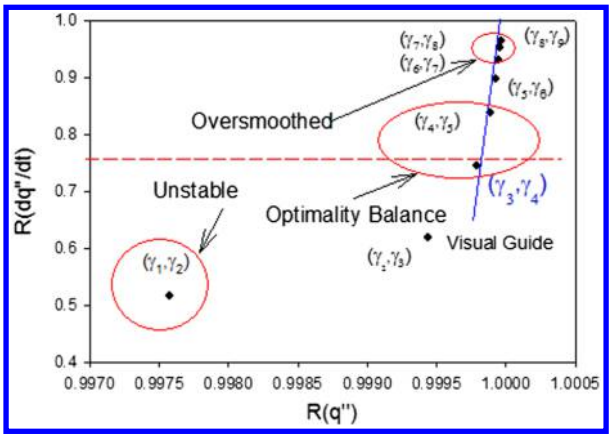

Fig. 8 Cross-correlation phase plane for the noisy results.

All three solutions qualitatively show similar reconstructions of the heat flux step.

IV. Conclusions

The preconditioned integral formulation has been successfully applied to a synthetic case of a diamond-based calorimeter gauge tested in a reflected shock tunnel. The results show that the method can be accurately applied and the optimal regularization parameter can be predicted with the presence of experimentally representative noise. The formulation presented here lends itself to future studies where large temperature rises necessitate the inclusion of temperature-dependent thermophysical properties of the diamond.

Acknowledgments

The work reported here was supported by a grant provided to J. I. Frankel by the U.S. National Science Foundation (NSF-CBET-1703442) and by a grant from the U.K. Engineering Physical Sciences Research Council (EP/N009037/1).

References

[1] Geraets, R. T. P., McGilvray, M., Doherty, L. J., Morgan, R. G., James, C. M., and Buttsworth, D. R., "Development of a Fast-Response Calorimeter Heat Transfer Gauge," *Journal of Thermophysics and Heat Transfer*, Vol. 34, No. 1, 2020, pp. 193–202. https://doi.org/10.2514/1.T5688

[2] MacLean, M., and Holden, M., "Catalytic Effects on Heat Transfer Measurements for Aerothermal Studies with CO2," *44th AIAA Aerospace Sciences Meeting and Exhibit*, AIAA Paper 2006-0182, Jan. 2006. https://doi.org/10.2514/6.2006-182

[3] Palmer, R., and Morgan, R., "Stagnation Point Heat Transfer in Superorbital Expansion Tubes," *35th Aerospace Sciences Meeting and Exhibit*, AIAA Paper 1997-0280, Jan. 1997. https://doi.org/10.2514/6.1997-280

[4] Geraets, R. T. P., "Development and Testing of a Fast-Response Diamond Calorimeter Heat Transfer Gauge," Ph.D. Thesis, Univ. of Oxford, Oxford, England, U.K., 2020.

[5] Schultz, D. L., and Jones, T. V., "Heat Transfer Measurements in Short-Duration Hypersonics Facilities," NATO AGARD-AG-165, Paris, 1973.

[6] Frankel, J., Keyhani, M., and Elkins, B., "Surface Heat Flux Prediction Through Physics-Based Calibration, Part 1: Theory," *Journal of Thermophysics and Heat Transfer*, Vol. 27, No. 2, 2013, pp. 189–205. https://doi.org/10.2514/1.T3917

[7] Frankel, J. I., and Chen, H. C., "Heat Flux Data Reduction Using a Preconditioning Trial Function," *Journal of Thermophysics and Heat Transfer*, Vol. 34, No. 1, 2020, pp. 109–120. https://doi.org/10.2514/1.T5744

[8] Graebner, J., "Measurements of Specific Heat and Mass Density in CVD Diamond," *Diamond and Related Materials*, Vol. 5, No. 11, 1996, pp. 1366–1370. https://doi.org/10.1016/0925-9635(96)00550-X

[9] Beck, J. V., Blackwell, B., and St. Clair, C. R., Jr., *Inverse Heat Conduction*, Wiley, New York, 1985, pp. 1–50.

[10] Frankel, J. I., and Keyhani, M., "Phase-Plane Analysis and Cross-Correlation for Estimating Optimal Regularization Parameters in

Inverse Heat Conduction Problems," *Journal of Thermophysics and Heat Transfer*, Vol. 28, No. 3, 2014, pp. 542–548. https://doi.org/10.2514/1.T4357

[11] Churchill, R. V., and Brown, J. W., *Fourier Series and Boundary Value Problems*, McGraw–Hill, New York, 1978, pp. 46–116.

[12] Calvetti, D., Morigi, S., Reichel, L., and Sgallari, F., "Tikhonov Regularization and the L-Curve for Large Discrete Ill-Posed Problems," *Journal of Computational and Applied Mathematics*, Vol. 123, Nos. 1–2, 2000, pp. 423–446. https://doi.org/10.1016/S0377-0427(00)00414-3